M1-IRELE

ELEC-H401 Modulation and coding

DVB-C project

Authors :

Arico Amaury

Colot Emmeran

Professor :

Horlin François

Academic year :

2024 - 2025

Contents

Introduction

This report aims to complete the code that simulates a DVB-C transmission chain in matlab. It provides additionnal information from the theoretical part of the project.
The first part builds the transmission chain and link the blocks together such that the received signal is the same as the one transmitted (in a noiseless case).

Second part to be explained later

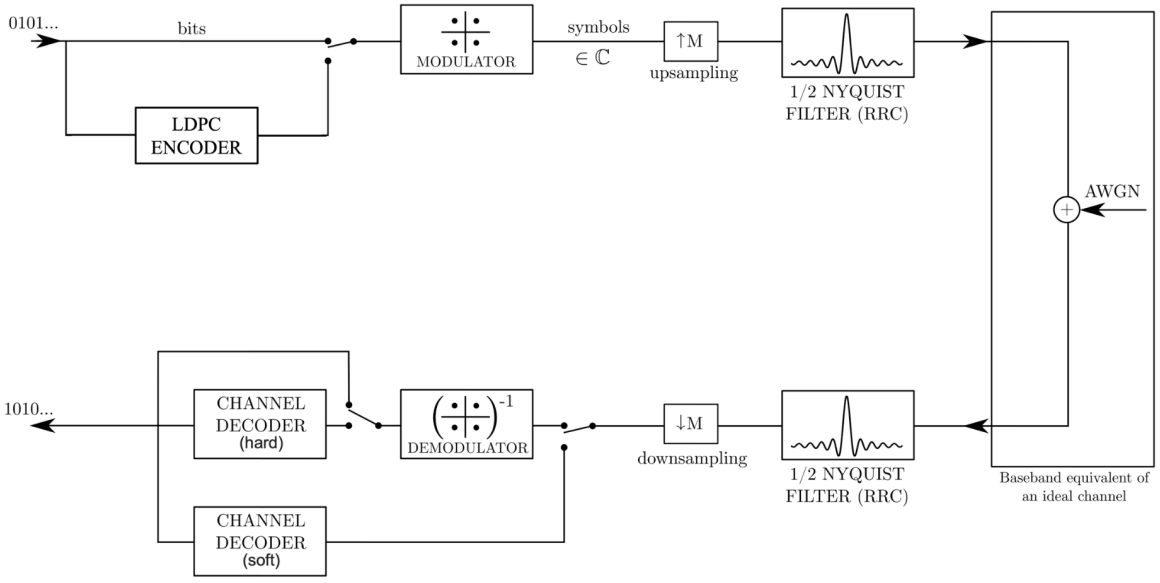

Figure 1: DVB-C transmission chain

Baseband representation

By looking at the block diagram of the transmission chain 1, one can see we never move the baseband signal to the carrier frequency. As the simulation runs on a computer, using the bandpass representation of the signal would require much more samples as the sampling frequency would need to be at least twice the carrier frequency. By simulating the chain in baseband, the minimal sampling frequency is reduced to the symbol rate in order to have at least one sample per symbol.
Because the signal is oversampled, the sampling frequency is then equal to the symbol rate multiplied by the oversampling factor.

Modulation and Demodulation

After generating N random bits, they are modulated. This allows to send fewer symbols than the number of bits. We chose QAM modulation as it combines ASK and PSK. Depending on the number of bits per symbol (N_{bps}), the number of bits sent (N) had to be chosen such that $N/N_{\text{bps}} \in \mathbb{N}$.
Figure 2 compares the constellation diagrams obtained for QAM-16 and QAM-64. As the constellations points are more spaced on the left, QAM-16 is less prone to a wrong demodulation (when noise will be added). This comes at the cost of a lower bitrate: for the same symbol rate, QAM-64 will send 6 bits while QAM-16 only send 4. It clearly shows a compromise between reliability and capacity.

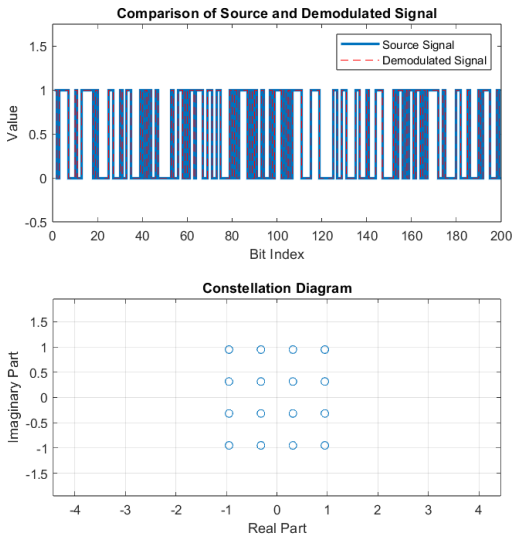

(a) QAM-16 modulation

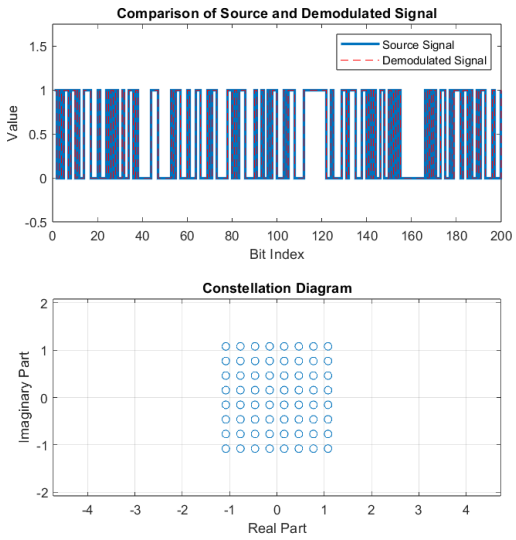

(b) QAM-64 modulation

Figure 2: Comparison of QAM modulations, where the mean square error is computed between the transmitted and received bitstream

Optimal demodulator and detector

First, it is important to remind that the transmitted signal is represented by a set of coefficients which results from the projection of the signal on an orthonormal basis related to the chosen modulation. Once transmitted, the signal is affected by noise (AWG noise here). In the general case, this noise moves the signal, resulting in a change in its coefficient in the basis, as can be seen on Figure 3

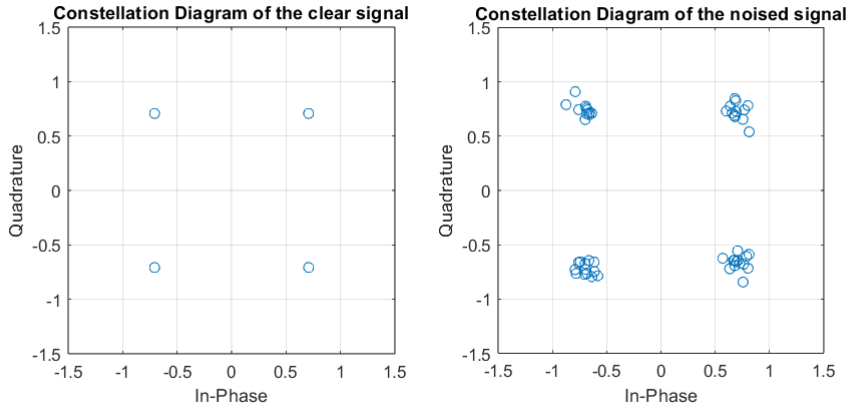

Figure 3: Effect of noise on the constellation diagram

To construct an optimal demodulator, 2 criteria should be taken into account. The first one is the sufficient statistic criteria. It is proven that once the received signal is projected on the sub-space defined by the previous basis functions, the noise component outside of the sub-space is independent from the pro-

jected signal. It means that there is no information loss when projecting the received signal on the original sub-space and the optimal decision can therefore be made using the projection of the incoming signal.

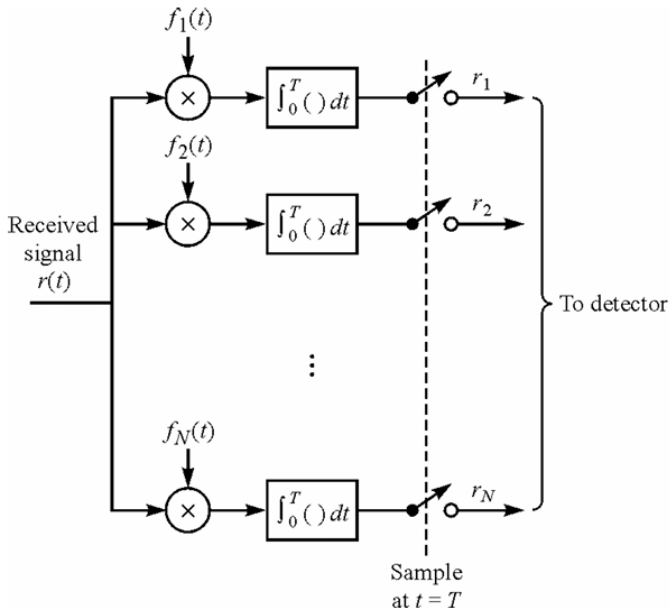

Figure 4: Projection on basis sub-space

$$
\begin{aligned}
E\left[n'(t)r_k\right] &= E\left[n'(t)\right]s_{mk} + E\left[n'(t)n_k\right] \\
&= E\left[n'(t)n_k\right] \\
&= E\left[\left(n(t) - \sum_{l=1}^{K} n_l f_l(t)\right) n_k\right] \\
&= \int_{t'=-\infty}^{\infty} E\left[n(t)n(t')\right] f_k(t')dt' - \sum_{l=1}^{K} E\left[n_l n_k\right] f_l(t) \\
&= \frac{N_0}{2} f_k(t) - \frac{N_0}{2} f_k(t) = 0
\end{aligned}
$$

Figure 5: Criteria of sufficient statistics

The second criteria is the usage of matched filters. The demodulator used to achieve the sufficient statistic property is composed of a bank of correlators (projection on a basis function). Instead of using a bank of correlators, we can use a bank of filters matched to the basis functions of the chosen modulation. It is proven that such filters at the demodulator gives a maximized SNR (minimize the power of the noise at the exit of the demodulator).

In conclusion, by using a bank of filters matched on the orthonormal basis function set by the choice of the modulation, we can construct a optimal demodulator which will ensure an optimal decision based on the received signal and ensure a maximum SNR at the output of this demodulator.

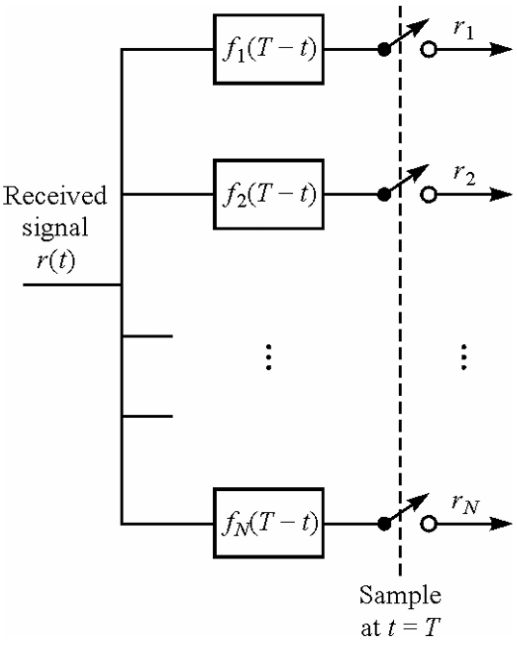

Figure 6: Bank of filters matching basis functions

$$\text{SNR} := \frac{\left[\int_{\tau=-\infty}^{\infty} s(\tau)h(-\tau)d\tau\right]^2}{\frac{N_0}{2}\int_{\tau=-\infty}^{\infty} h^2(-\tau)d\tau}$$

Cauchy-Schwartz inequality:

$$\left[\int_{t=-\infty}^{\infty} g_1(t)g_2(t)dt\right]^2 \leq \int_{t=-\infty}^{\infty} g_1^2(t)dt \int_{t=-\infty}^{\infty} g_2^2(t)dt$$

Equality if $g_1(t) = kg_2(t)$ for any arbitrary constant k

Figure 7: Maximum SNR demonstration

At the output of the demodulator, we still need to make sure the optimal choice of the M possible $s_m(t)$ is made based on the received signal. To achieve this, the maximum likelihood criteria is used. It is equivalent to the maximum a posteriori criteria (general criteria) in the case of equiprobable symbols $s_m(t)$. The criteria leads to the following result : the optimizal $s_m(t)$ choice is found by taking the minimum euclidian distance between the observable received signal $r(t)$ and all the possible modulated signal $s_m(t)$.

Pulse shaping

With modulation only, the bandwidth of the transmitted signal is infinite. This is problematic as it could interfere with neighboring channels. A filtering is applied to resolve this but the chosen filter must respect two other constraints: it must cancel inter-symbol interference (ISI) and must maximize the SNR.
The raised cosine filter is chosen as it limits the bandwidth and cancels ISI. To maximize the SNR, it is applied as a matched filter by using the square root of it at the transmitter and at the receiver.
The time domain and frequency domain representation of the raised cosine filter is shown in Figure 8. Figure 9 shows how the signal is shaped in the time domain and how there is indeed no ISI. Finally, the power spectral density [1] of the transmitted signal is plotted in figure 10 where the frequency band is limited to $[-3,3]$MHz.

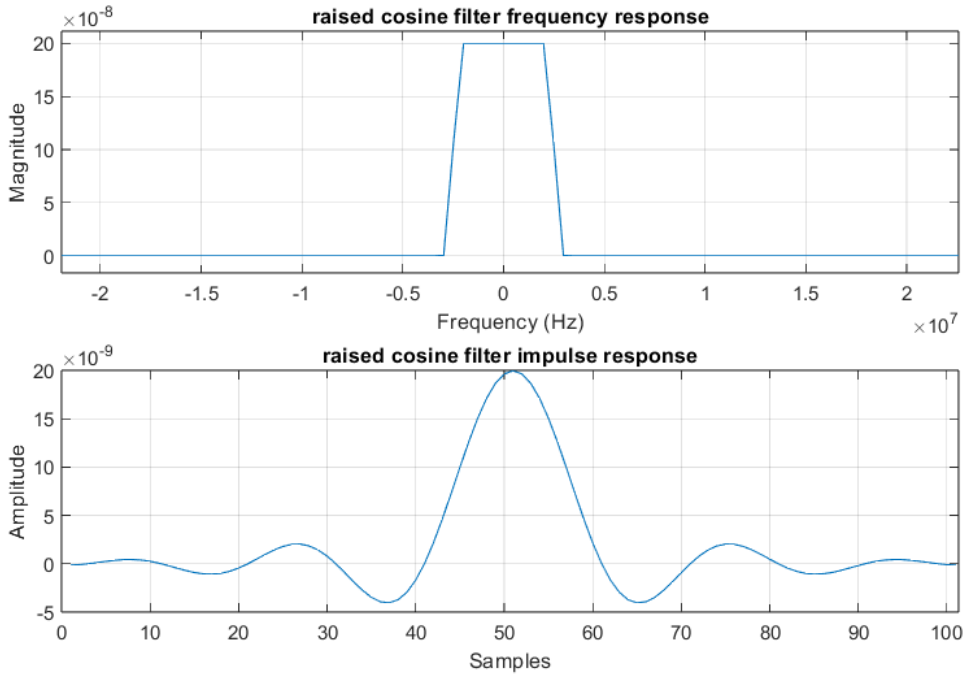

Figure 8: Time and frequency domain representation of the raised cosine filter

[1] PSD as the signal is a random variable

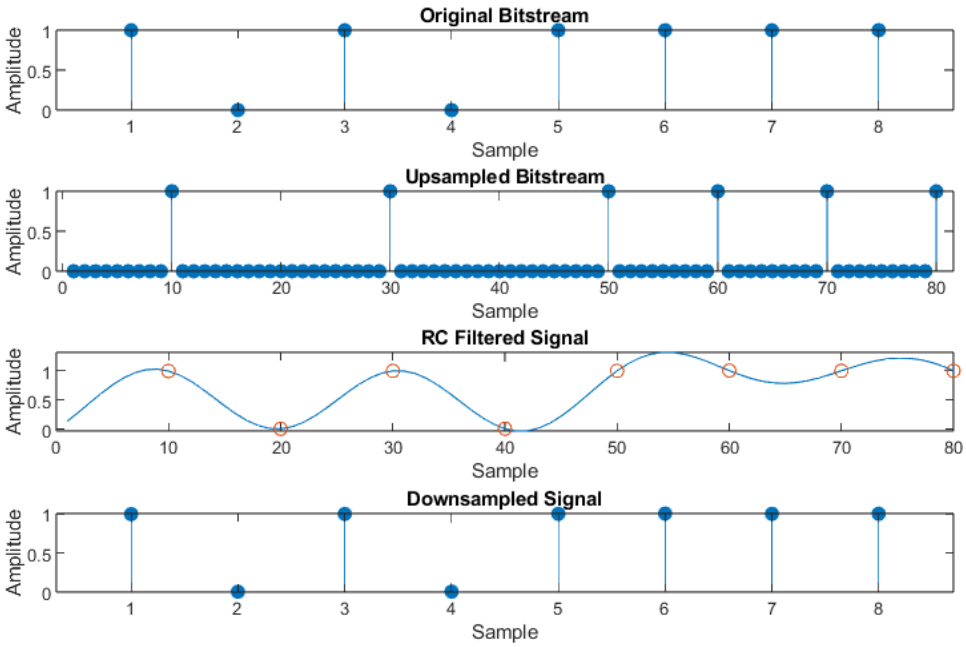

Figure 9: Pulse shaping with a raised cosine filter

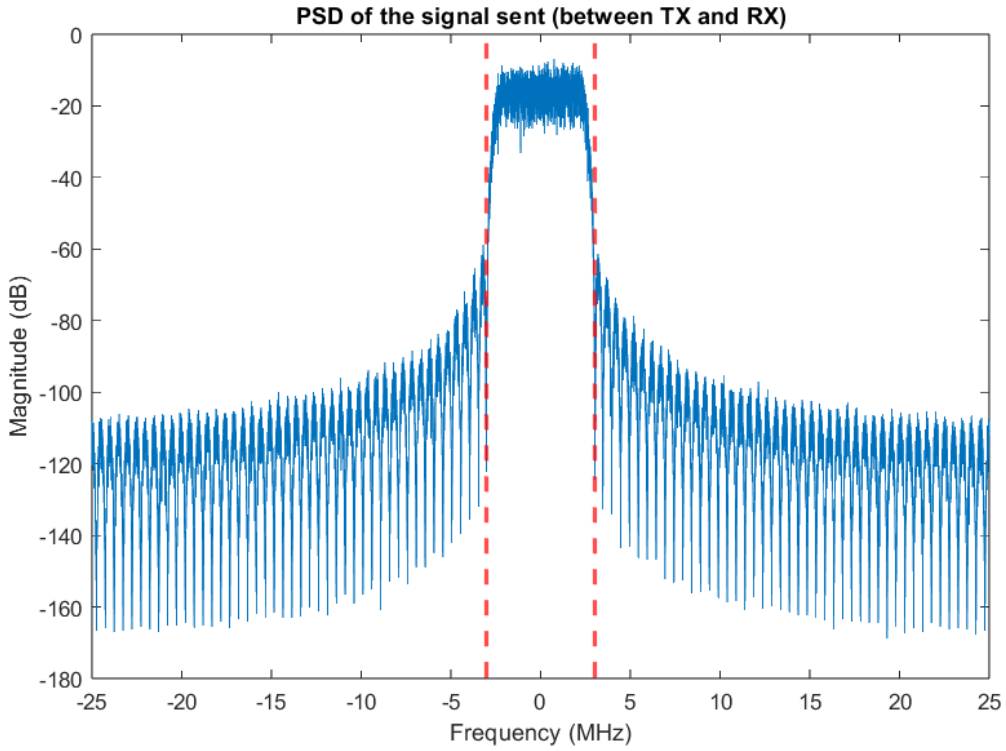

Figure 10: PSD of the transmitted signal after pulse shaping

Noise addition

The last building block is a noise source. It generates additive white Gaussian noise in baseband. When the signal is too much corrupted, the demodulation can fail. The BER curves are plotted in figure 11 and they show the impact of the noise power N_0 on the bit error rate. The compromise between reliability and capacity is again visible: in the same conditions (same E_b/N_0), a modulation with lower capacity will have a smaller BER.

The theoretical BER curves are plotted on figure 11 and are compared with the simulation results. They stay close to each other untill the BER reaches 10^{-4}. This limit could go even lower by increasing the number of bits sent but we limited it to 10^6 in order for the code to run quite fast.

To impose a value of E_b/N_0, we start by computing the energy of the transmitted signal before adding the noise. The power of the noise is then chosen as $N_0 = E_b/(E_b/N_0)_{\text{desired}}$.

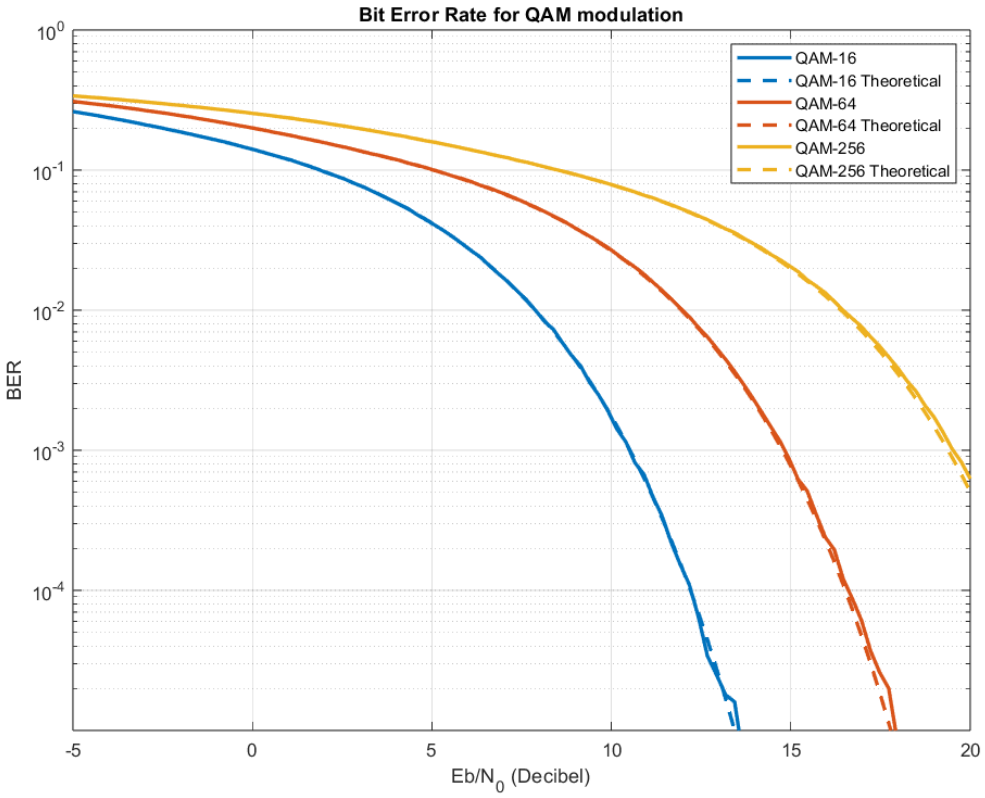

Figure 11: BER curves for different QAM modulations

Bit rate

Considering the following characteristics :

- (a) Physical bandwidth of $B_{\text{physical}} = 6$ MHz
- (b) Roll-off factor $\beta = 0.2$
- (c) QAM 16 modulation $\rightarrow$ Nbps = 4

We can derive the symbol rate from the physical bandwidth

$$f_{\text{symbol}} = \frac{B_{\text{physical}}}{1+\beta} = 5MHz$$

$$\text{Bit-rate} = f_{\text{symbol}} * \text{Nbps} = 5\text{MHz} * 4 = 20\text{MBps}$$

Description

Because the receiver and transmitter are not at the same location, the carrier frequencies and the samplers at TX and RX will have a different phase and due to the inaccuracies of the oscillator, the frequencies will also be slightly different.
This is summarized in 4 effects:

- **Carrier frequency offset (CFO)**: The difference in the carrier frequencies at TX and RX ($= \Delta\omega$). It will add ISI as the RRC are not anymore matched and a linearly increasing phase shift will appear.
- **Phase offset**: The difference between the phase of the carrier signal at TX and RX.
- **Sampling frequency offset (SFO)**: The difference in the sampling frequencies at TX and RX.
- **Time shift**: The difference in the timing of the samples at TX and RX.

Implementation

CFO

The CFO implementation is done by multiplying the signal with a complex exponential $e^{j2\pi\phi_{\text{ppm}} f_c t}$. The phase offset is added to the CFO. It is defined in ppm (part per million) where the ppm value is $\frac{\Delta\omega}{f_c} 10^{-6}$.
Figure 12 shows the BER curves with different CFO values. In order to have useful results, the linear phase shift is removed right after the second RRC filter. This allows to only keep the effect of ISI on the BER curve.

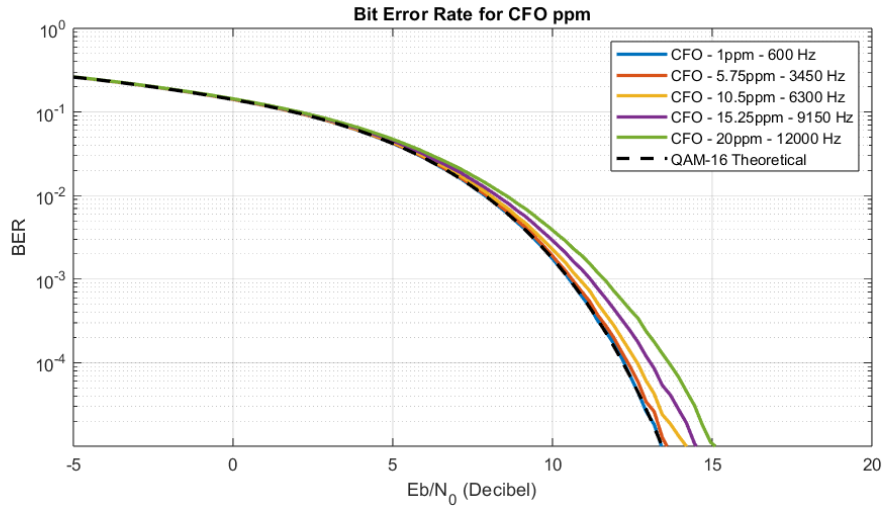

Figure 12: BER with different CFO values

Figure 13 shows the effect of CFO on the symbol constellation for QAM-16. It is here plotted without any noise and with parameters that allow us to see the line phase shift of the symbols.

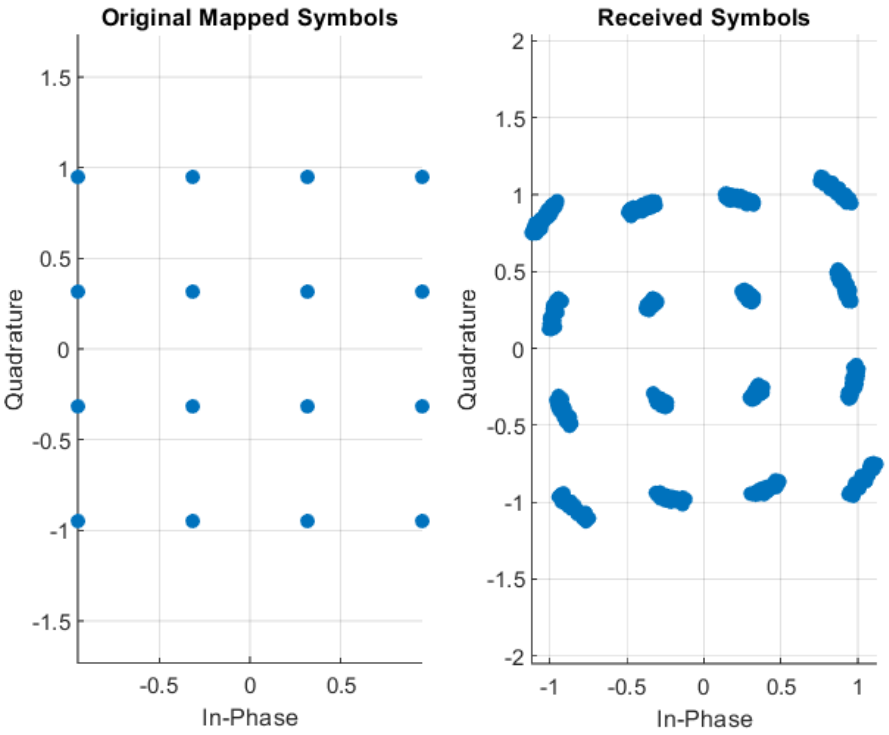

Figure 13: Constellation before and after CFO

Phase offset

The same is done for the phase offset where the exponential is simply $e^{j\phi}$ where ϕ is chosen once at the begining of the simulation.

The effect of the phase offset is only visible on the constellation plot (figure 14) where every point is rotated by a fixed angle (whereas CFO rotated the symbols linearly with time).

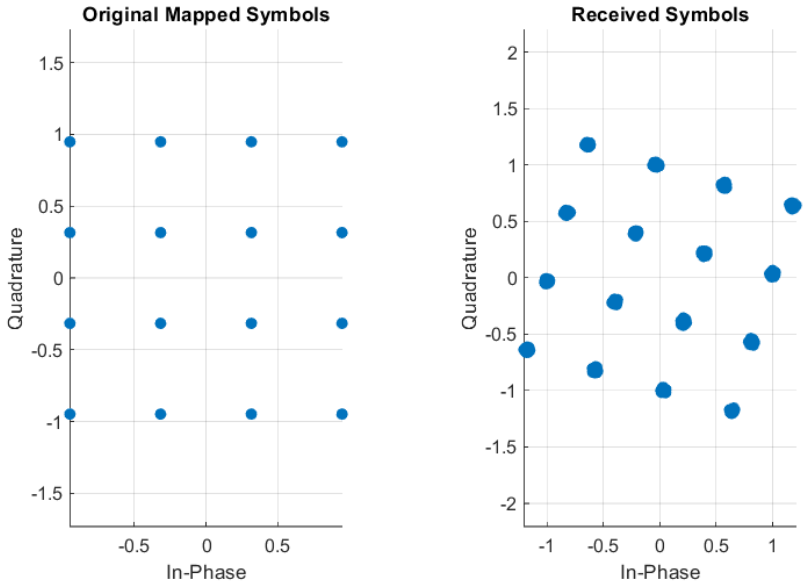

Figure 14: Constellation before and after phase offset

On a BER curve (figure 15), the phase is not visible as from the errors originating from the phase offset are either on every symbol or on none and this is why the error does not depend anymore on E_b/N_0.

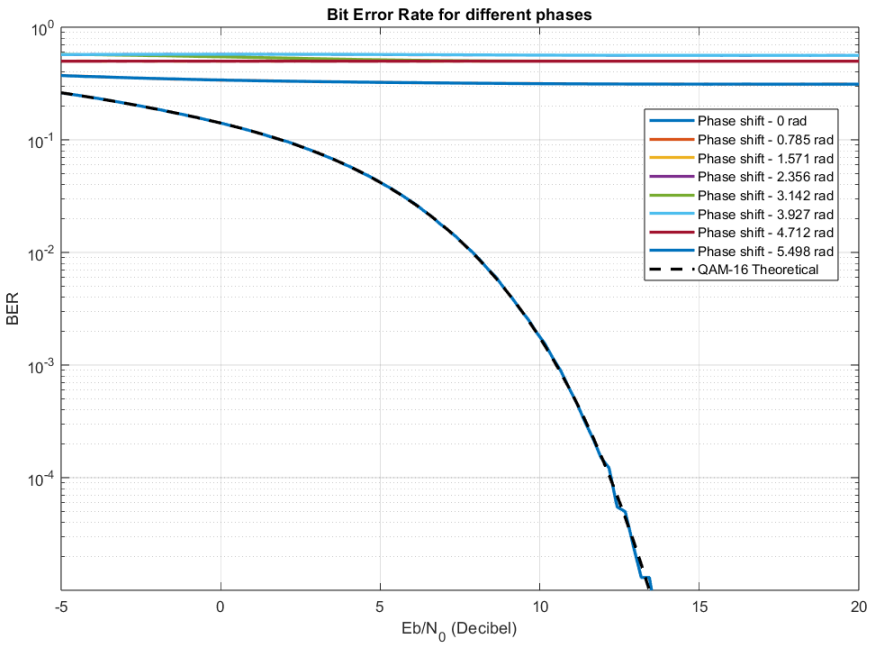

Figure 15: BER with phase offset

SFO

The SFO is neglected in the simulation as it would need some interpolation and more complex computations.

Time shift

The time shift is implemented by simply shifting the samples in the array with an oversampling factor that is large enough.

A larger time shift will increase the BER as the samples will be taken at the wrong time. For sufficiently low values, it will still behave as a "classical" BER curve but from some point, there is just no more correlation between the measured sample and the received one and the BER tends to a 0.5 line, as shown in figure 16.

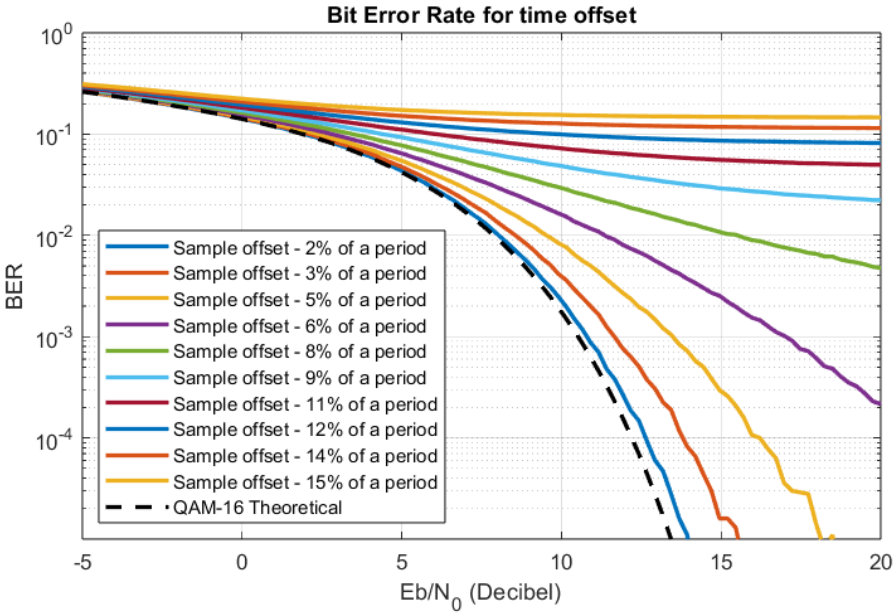

Figure 16: BER with time shift

Correction

Frame and frequency acquisition

With the previous correction, the receiver knows when to sample but there still is some uncertainty on the frequency. The way to remove the CFO is to send in the data a known pilot and the first step is to detect when this pilot is received. This is known as frame acquisition and it is performed with the differential cross-correlator:

$$D_k[n] = \frac{1}{N-k} \sum_{l=k}^{N-1} \left(y^*[n+l]a[l]\right)\left(y^*[n+l-k]a[l-k]\right)^*$$

Where a is the known pilot, N its length and k the delay between the two correlations.

$D_k[n]$ is computed for every time index n and for every shift k until its maximum value, K. The estimation of the index of the start of the frame $\hat{n}$ and the estimation of the CFO $\hat{\Delta f}$ are given by:

$$\hat{n} = \arg\max_n \sum_{k=1}^{K} |D_k[n]|$$

$$\hat{\Delta f} = -\frac{1}{K} \sum_{k=1}^{K} \frac{\angle D_k[\hat{n}]}{2\pi k T}, \qquad T \text{ being the symbol duration.}$$

The implementation of the time of arrival estimator has been done on figure 17 by placing the pilot at the 100th sample and by then plotting $\sum_{k=1}^{K} |D_k[n]|$. The peak at the 100th sample clearly indicates the time of arrival of the pilot and validates the implementation. A similar test was done for the CFO estimation but it is not shown here.

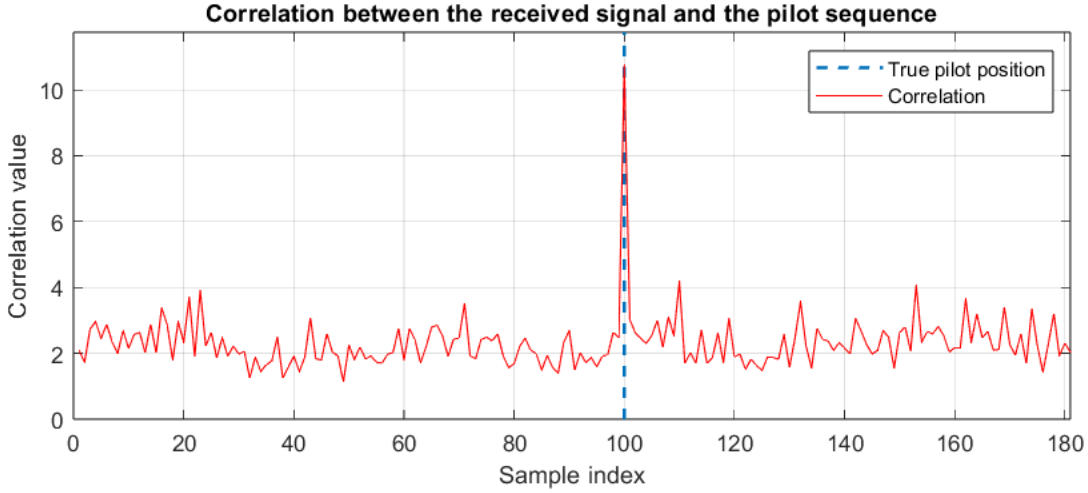

Figure 17: Time of arrival estimation

The standard deviation of both estimators has been mesured on 250 runs for both a varying pilot length N and a varying maximal shift K for an increasing $\frac{E_b}{N_0}$ in figures 18 and 19.

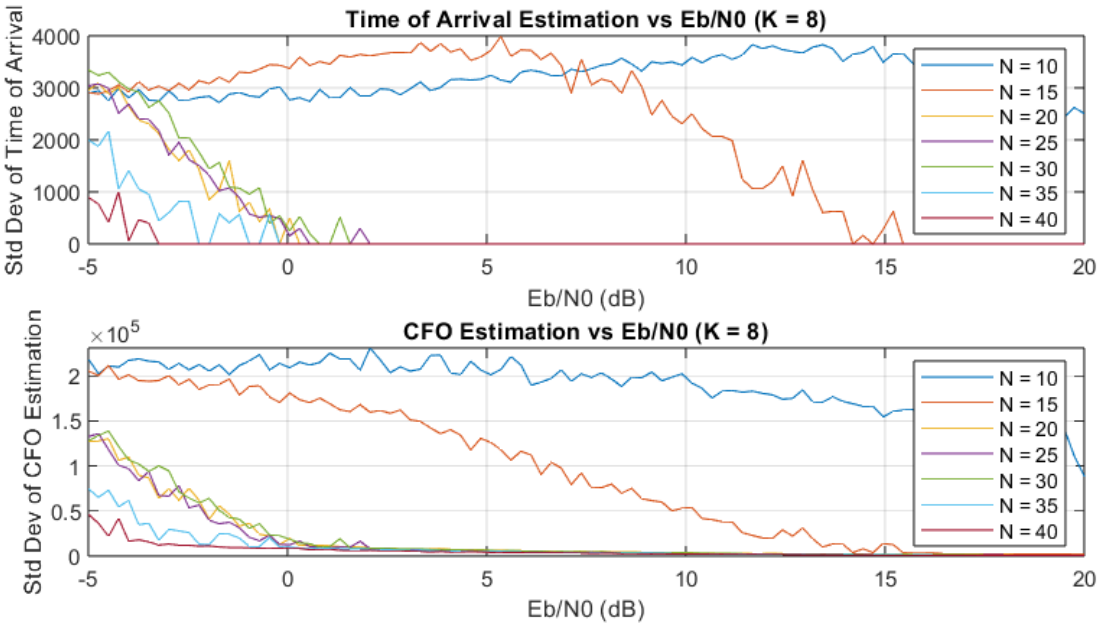

Figure 18: Standard deviation of the CFO estimator with varying pilot length

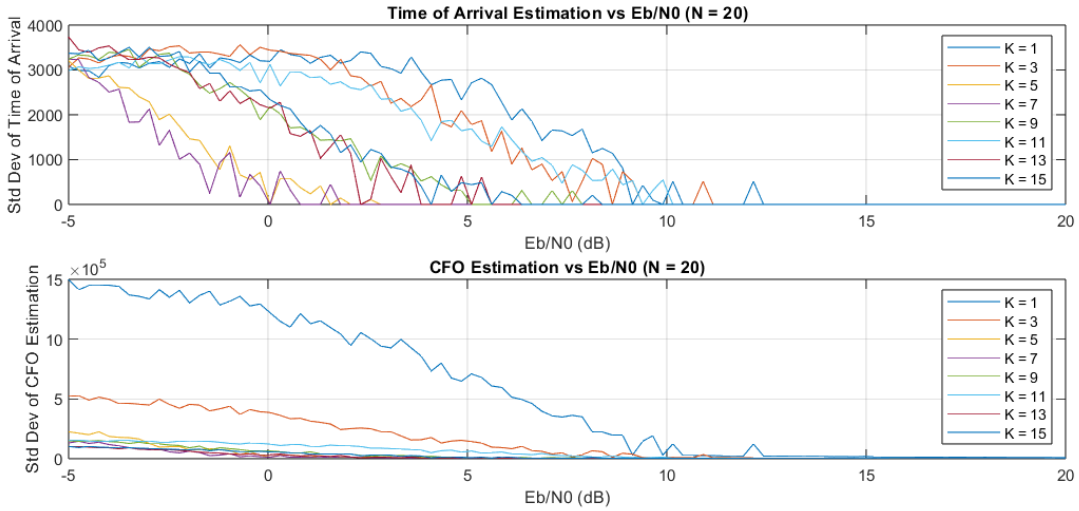

Figure 19: Standard deviation of the CFO estimator with varying maximal shift

As expected, a longer pilot and a larger shift will lower the uncertainty of the estimation and the same goes by for an increasing SNR.

The robustness of the frame acquisition is also tested against a varying CFO.